Integrated Flight Control Design for a Large Flexible Aircraft

Julian Theis, Harald Pfifer, Gary Balas and Herbert Werner

***Abstract*— A systematic design procedure suited to integrate rigid body and aeroelastic control objectives within the mixed sensitivity framework is proposed for a two-degrees-of-freedom control configuration. It is based on a modal representation and combines stability augmentation, structural mode control and maneuver demand in a single linear parameter-varying (LPV) controller. To demonstrate applicability, an integrated flight control system is designed for the nonlinear model of a large flexible aircraft. The integrated controller is shown to greatly reduce structural vibrations while maintaining handling qualities and robustness margins of a conventional controller.**

I. Introduction

Active aeroelastic control becomes an increasingly important aspect of flight control for large aircraft. Weight reduction and aerodynamically efficient design characteristics such as slender fuselages and high aspect ratio wings reduce structural stiffness of the airframe. Hence, structural deformations occur at low frequencies and can cause undesired coupling with rigid body dynamics. Consequently, adverse aeroelastic effects are receiving increased attention within the aerospace community, see, e. g., [1], [2], [3].

With the advent of fly-by-wire, including objectives such as reduction of structural vibrations, ride quality enhancement and gust load alleviation into the flight control system (FCS) has become feasible. A strict frequency separation of the individual control systems is prevalent to avoid excitation of structural modes by the primary FCS and interference of the secondary FCSs with handling qualities. This is usually achieved through the use of complementary filtering, a strategy not valid in case that elastic and rigid body modes are close in frequency. Classical flight control further depends largely on one-loop-at-a-time design procedures and cascaded layers of control systems, [4]. The inner loops provide desirable dynamic behavior and are known as stability augmentation systems (SASs). They are usually gain-scheduled so that the augmented dynamics remain almost constant across the flight envelope and thus provide "dynamics equalization", [5]. Structural mode control systems (SMCSs), dedicated to the reduction of aeroelastic vibrations, form a second inner-loop. Outer loops for maneuver demand and autopilot functions are then concatenated on the inner loops. This separation prevents the conventional control surfaces from engaging in aeroelastic control and surplus effectors from aiding in rigid body control.

Julian Theis and Herbert Werner are with the Institute of Control Systems, Hamburg University of Technology, Hamburg, Germany. {julian.theis, h.werner}@tuhh.de

Harald Pfifer is and Gary Balas was with the Aerospace Engineering and Mechanics Department, University of Minnesota, Minneapolis. hpfifer@umn.edu

The potential benefits of an integrated control system that jointly uses available effectors are believed to be significant and thus several researchers have addressed the design problem. Often μ-synthesis (see, e. g., [6]) is employed since the multiple performance and robustness criteria for flight control are difficult to formulate in an unstructured description. For instance, in [7], integration of stability augmentation and maneuver demand in a two-degrees-of-freedom architecture (so-called superaugmented control) is considered. An approximate μ-synthesis is used within the linear parameter-varying (LPV) framework and design studies are performed for rigid body aircraft. An integrated control approach for a flexible aircraft is described in [8], where a gain-scheduled SAS for dynamics equalization is designed to facilitate the use of a single linear time invariant (LTI) μ-synthesis controller in an outer loop to reduce aeroelastic vibrations. A one step approach for integrated control of a flexible aircraft, again using an approximate μ-synthesis within the LPV systems framework, is shown to be beneficial compared to a sequential design in [9]. Despite the success of these integration attempts, μ-synthesis remains theoretically limited to LTI systems and potentially leads to very high order controllers unsuitable for implementation.

The present paper seeks to combine the aforementioned integration steps—stability augmentation, maneuver demand and aeroelastic control—into a fully integrated multivariable LPV control strategy without relying on approximate μ-synthesis. It contributes systematic design guidelines by means of a detailed design study. As a representative example, a model of the Rockwell B-1 Lancer [10] is used (Section III). The aircraft had serious ride quality issues due to adverse aeroelastic effects causing structural vibrations at the cockpit. This necessitated the incorporation of a dedicated SMCS using additional canards located close to the cockpit as effectors, [11]. In the present paper, an integrated LPV controller is designed for the lateral-directional dynamics in Section IV and evaluated in nonlinear simulation against a classical SAS+SMCS architecture in Section V.

II. Linear Parameter-Varying Systems

LPV systems are a class of dynamic systems whose state space representations depend continuously on a time-varying scheduling parameter vector $\rho\colon \mathbb{R} \mapsto \mathcal{P}$, where $\mathcal{P} \subset \mathbb{R}^{n_\rho}$ is a compact set of allowable parameters. Additionally, the parameter rates $\dot{\rho}\colon \mathbb{R} \mapsto \mathcal{V}$ are restricted to lie in a polyhedron $\mathcal{V} = \{\dot{\rho} \in \mathbb{R}^{n_\rho} \mid |\dot{\rho}_i| \leq \nu_i \ , \quad i = 1, \ldots, n_\rho\}$ and hence the set of all admissible parameter trajectories is $\mathcal{A} = \{\rho(t) \mid \rho(t) \in \mathcal{P} \wedge \dot{\rho}(t) \in \mathcal{V} \quad \forall t \in \mathbb{R}\}$. The continuous matrix functions $A\colon \mathcal{P} \mapsto \mathbb{R}^{n_x \times n_x}$, $B\colon \mathcal{P} \mapsto \mathbb{R}^{n_x \times n_w}$,

$C\colon \mathcal{P} \mapsto \mathbb{R}^{n_z \times n_x}$, $D\colon \mathcal{P} \mapsto \mathbb{R}^{n_z \times n_w}$, the state $x\colon \mathbb{R} \mapsto \mathbb{R}^{n_x}$, input $w\colon \mathbb{R} \mapsto \mathbb{R}^{n_w}$, and output $z\colon \mathbb{R} \mapsto \mathbb{R}^{n_z}$ constitute a state space model

$$G_\rho\colon \begin{cases} \dot{x}(t) = A(\rho(t))\ x(t) + B(\rho(t))\ w(t) \\ z(t) = C(\rho(t))\ x(t) + D(\rho(t))\ w(t)\ . \end{cases} \tag{1}$$

The dependence on parameters and time is from now on occasionally dropped to shorten notation.

A common way to obtain such an LPV model is to linearize a nonlinear system with respect to a continuum of assumed constant equilibrium points defined by $\mathcal{A}$. The resulting model describes the local behavior about each equilibrium but is only an approximation of the original nonlinear system, see [12], [13]. Using the LPV framework allows to systematically extend robust control techniques such as $\mathcal{H}_\infty$-norm optimal design (see e. g. [6]) to nonlinear systems that can be approximated as in (1). To this end, the induced $\mathcal{L}_2$-norm of an LPV system (1) is defined as

$$\|G_\rho\| = \sup_{w \in \mathcal{L}_2 \setminus \{0\},\ \rho \in \mathcal{A},\ x(0)=0} \frac{\|z\|_2}{\|w\|_2}\ . \tag{2}$$

A controller that satisfies performance specifications in terms of this norm can be synthesized with the following result:

Theorem 1 ([14], [15]): Let $\mathcal{A}$ be a compact set and

$$P_\rho\colon \left\{ \begin{bmatrix} \dot{x} \\ e_1 \\ e_2 \\ y \end{bmatrix} = \begin{bmatrix} A & B_{11} & B_{12} & B_2 \\ C_{11} & D_{1111} & D_{1112} & 0 \\ C_{12} & D_{1121} & D_{1122} & I \\ C_2 & 0 & I & 0 \end{bmatrix} \begin{bmatrix} x \\ d_1 \\ d_2 \\ u \end{bmatrix} \right. \tag{3}$$

be an open loop LPV system whose special structure can be achieved through loop-shifting and scalings under mild conditions, see [16]. Denote $C_1^T = \left[\, C_{11}^T\ C_{12}^T \,\right]$, $B_1 = \left[\, B_{11}\ B_{12} \,\right]$, and $\left[\begin{smallmatrix} D_{111\bullet} \\ D_{112\bullet} \end{smallmatrix}\right] = \left[\begin{smallmatrix} D_{1111}\ D_{1112} \\ D_{1121}\ D_{1122} \end{smallmatrix}\right] = \left[\, D_{11\bullet 1}\ D_{11\bullet 2} \,\right]$. There exists an LPV output feedback controller

$$K_\rho\colon \begin{cases} \dot{x}_K(t) = A_K(\rho(t))\ x_K(t) + B_K(\rho(t))\ y(t) \\ u(t) = C_K(\rho(t))\ x_K(t) + D_K(\rho(t))\ y(t) \end{cases} \tag{4}$$

that internally stabilizes the closed-loop interconnection given by the lower fractional transformation $\mathcal{F}_L(P_\rho, K_\rho)$ and guarantees $\|\mathcal{F}_L\left(P_\rho, K_\rho\right)\| < \gamma$ if there exist symmetric positive definite matrix functions $X\colon \mathcal{A} \mapsto \mathbb{R}^{n_x \times n_x}$ and $Y\colon \mathcal{A} \mapsto \mathbb{R}^{n_x \times n_x}$ such that for all $\rho \in \mathcal{A}$

$$\begin{bmatrix} X & \frac{1}{\gamma} I \\ \star & Y \end{bmatrix} \succ 0 \tag{5a}$$

$$\begin{bmatrix} \Lambda_X - B_2\, B_2^T & X\, C_{11}^T & \frac{1}{\gamma}\left(B_1 - B_2\, D_{112\bullet}\right) \\ \star & -I & \frac{1}{\gamma}\, D_{111\bullet} \\ \star & \star & -I \end{bmatrix} \prec 0 \tag{5b}$$

$$\begin{bmatrix} \Lambda_Y - C_2^T\, C_2 & Y\, B_{11} & \frac{1}{\gamma}\left(C_1^T - C_2^T\, D_{11\bullet 2}^T\right) \\ \star & -I & \frac{1}{\gamma}\, D_{11\bullet 1}^T \\ \star & \star & -I \end{bmatrix} \prec 0 \tag{5c}$$

where $M \succ (\prec)\, 0$ denotes M is positive (negative) definite, $\Lambda_X = X\ (A - B_2\, C_{12})^T + (A - B_2\, C_{12})\ X - \sum_{i=1}^{n_\rho} \frac{\partial X}{\partial \rho_i}\, \dot{\rho}_i$, $\Lambda_Y = Y\ (A - B_{12}\, C_2) + (A - B_{12}\, C_2)^T\ Y + \sum_{i=1}^{n_\rho} \frac{\partial Y}{\partial \rho_i}\, \dot{\rho}_i$, and $\star$ denotes symmetric completion.

Such a controller can be constructed by closed formulae from the open loop plant matrices and the feasible values of X, Y, and γ as given in [14]. It is then usually implemented in a lookup table representation with linear interpolation. Since the constraints (5) in Theorem 1 are infinite dimensional, a common approach is to approximate the admissible space by a finite dimensional set $\{p_k\}_1^{n_{\text{grid}}} \subset \mathcal{A}$, called a grid. This is also the natural form in which aeroelastic aircraft are modeled for different points within the flight envelope, with parameters typically being altitude and airspeed.

III. Model of a Large Flexible Aircraft

A nonlinear Matlab/Simulink simulation resembling the Rockwell B-1 Lancer aircraft (Fig. 1) was recently developed by David Schmidt from data available in the open literature and can be downloaded from [10]. It has sparked renewed interest in the B-1 as a benchmark example of an aeroelastic aircraft, see, e. g., [17]. The simulation model includes nonlinear rigid body dynamics, nonlinear quasi-steady aerodynamic data, actuator and servo models, as well as the three lowest-frequency symmetric and two lowest-frequency antisymmetric elastic deformation modes of the airframe. The generalized displacements of the elastic modes are denoted (E_1, E_2, E_3) for the symmetric and (E_4, E_5) for the antisymmetric deformation. E_1, E_3 and E_5 are mainly fuselage bending modes that contribute to vibrations at the cockpit, while E_2 and E_4 are primarily wing bending modes. The present paper is concerned with the lateral-directional dynamics that provide a challenging multivariable control problem.

A. Existing Control Structure

The existing control structure for the lateral dynamics consists of an SAS, active up to about 5 rad/s, and a dedicated SMCS, only active in a frequency range of about 5-30 rad/s. The SAS is formed of roll rate (p) damper, washed-out yaw rate (r) damper and lateral acceleration ($a_{y,\text{cg}}$) feedback for turn coordination. The effectors are the horizontal tail (δ_{DH}), wing upper-surface spoilers (δ_{sp}), as well as upper (δ_{RU}) and lower (δ_{RL}) split rudder. The SMCS employs the principle of

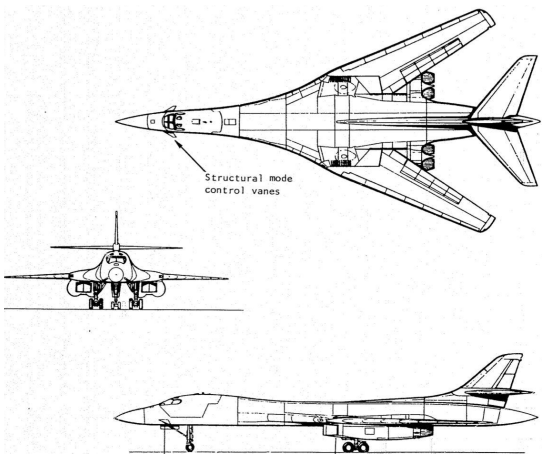

Fig. 1. Three-view of the Rockwell B-1 Lancer [11]

identical location of accelerometer and force [11] and generates forces opposing the current velocity to actively reduce vibrations at the cockpit, indicated by the lateral acceleration $a_{y,\text{cp}}$. It uses anti-symmetrically deflectable control vanes ($\delta_{\text{cv,anti}}$) at the cockpit as effectors.

B. Grid-based LPV Approximation

For control synthesis, the nonlinear model is linearized at a number of operating points in cruise condition, yielding the rectangular grid $Ma \times h = \{0.6, 0.7, 0.8\} \times \{5,000\,\text{ft}, 10,000\,\text{ft}, 15,000\,\text{ft}, 20,000\,\text{ft}\}$, where Ma denotes the Mach number and h the altitude. Rate bounds are selected as $|\dot{Ma}| < 0.1\,1/\text{s}$ and $|\dot{h}| < 1,000\,\text{ft/s}$ based on the study [17] concerned with the sensitivity of the existing control system to these dynamic variations. The complete lateral-directional model with 16 states contains bank angle, roll rate, yaw rate and lateral velocity dynamics, as well as the E_4 and E_5 elastic modes. The unstable spiral mode is removed by truncation after applying a common coordinate transformation to all grid points. Further, all actuator and servo dynamics with a bandwidth larger than 10 rad/s are neglected. Thus, the synthesis model $y = G_\rho\, u$ is stable and has 10 states. The output is $y = \begin{bmatrix} p & r & a_{y,\text{cg}} & a_{y,\text{cp}} \end{bmatrix}^T$ and the input $u = \begin{bmatrix} \delta_{\text{DH}} & \delta_{\text{RL}} & \delta_{\text{RU}} & \delta_{\text{sp}} & \delta_{\text{cv,anti}} \end{bmatrix}^T$.

IV. Control Design

The three main control objectives have very clear interpretations in terms of the system's stability modes. Good handling qualities are primarily achieved by providing additional damping to the dutch roll mode. Ride quality enhancement for the B-1 translates to vibration reduction at the cockpit and can be addressed via damping of the fuselage bending mode E_5. Structural loads are on the other hand primarily associated with the wing bending mode E_4. In the proposed design scheme, the generalized velocities associated with these modes are used for the definition of a mixed sensitivity problem both to attenuate structural modes and to increase handling qualities associated with the rigid body modes. The approach is adapted from [8] where it was introduced for the damping of structural modes represented by an LTI model.

A. Modal Representation

To define the modal velocities on the LPV model, the fixed-parameter LTI systems at each grid-point are transformed individually into modal form described by

$$\dot{\tilde{x}} = \begin{bmatrix} \tilde{A}_1 & 0 & & \\ 0 & \tilde{A}_2 & \ddots & \\ & \ddots & \ddots & 0 \\ & & 0 & \tilde{A}_n \end{bmatrix} \tilde{x} + \begin{bmatrix} \tilde{B}_1 \\ \tilde{B}_2 \\ \vdots \\ \tilde{B}_n \end{bmatrix} u \tag{6a}$$

$$y = \begin{bmatrix} \tilde{C}_1 & \tilde{C}_2 & \cdots & \tilde{C}_n \end{bmatrix} \tilde{x} + D\, u \tag{6b}$$

where $\tilde{A}_i = \left[\begin{smallmatrix} \Re(\lambda_i) & \Im(\lambda_i) \\ -\Im(\lambda_i) & \Re(\lambda_i) \end{smallmatrix}\right]$ for complex conjugate eigenvalues $\lambda_i = \Re(\lambda_i) \pm \mathrm{j}\,\Im(\lambda_i)$ and $\tilde{A}_i = \lambda_i$ for real eigenvalues. That is, the state space matrix A is transformed to Jordan real canonical form via a similarity transformation,

$$\tilde{A} = \tilde{\Phi} A\, \tilde{\Phi}^{-1}, \quad \tilde{\Phi} = \begin{bmatrix} \Re(v_1)\ \Im(v_1)\ \cdots\ \Re(v_n)\ \Im(v_n) \end{bmatrix}^{-1},$$

where v_i are the eigenvectors corresponding to the eigenvalues λ_i of the matrix A, see e. g. [18]. In this form, each of the decoupled subsystems ($\tilde{A}_i$, $\tilde{B}_i$, $\tilde{C}_i$) describes the dynamics of a stability mode and hence establishes physical interpretation of the system dynamics. The states associated with such a mode however lack physical interpretation. Therefore, a mode-wise transformation to a canonical second order system description is applied, i. e.,

$$\tilde{A}_i = \begin{bmatrix} -\omega_{0,i}\,\zeta_i & \omega_{d,i} \\ -\omega_{d,i} & -\omega_{0,i}\,\zeta_i \end{bmatrix} \overset{\bar{\Phi}_i}{\mapsto} \begin{bmatrix} 0 & 1 \\ -\omega_{0,i}^2 & -2\,\omega_{0,i}\,\zeta_i \end{bmatrix} = \bar{A}_i$$

where $\omega_{0,i}$ is the natural frequency of the mode, ζ_i is the corresponding damping ratio and $\omega_{d,i} = \sqrt{\omega_{0,i}^2\,(1-\zeta_i^2)}$ is the damped frequency. A permuted version of the multivariable controller canonical form construction scheme introduced in [18] is used and hence the transformation is described by

$$\bar{A}_i = \bar{\Phi}_i\, \tilde{A}_i\, \bar{\Phi}_i^{-1}, \qquad \bar{\Phi}_i = \begin{bmatrix} \varphi_i & \tilde{A}_i^T \varphi_i \end{bmatrix}^T,$$

where φ_i^T is the last row of $\begin{bmatrix} b_i & \tilde{A}_i\, b_i \end{bmatrix}^{-1}$ and b_i is the first column of $\tilde{B}_i$. In this form, the two states associated with the ith mode correspond to generalized displacement and generalized velocity $\begin{bmatrix} \eta_i & \dot{\eta}_i \end{bmatrix}^T$. The parameter dependence of the plant prohibits a global transformation to modal coordinates since a parameter-varying state transformation introduces rate-dependent dynamics, see e. g. [19]. Consequently, the matrices $\tilde{\Phi}$ and $\bar{\Phi}$ are used to define auxiliary outputs rather than state transformations and the plant output is augmented with $\eta = \begin{bmatrix} \eta_1 & \dot{\eta}_1 \cdots \eta_n & \dot{\eta}_n \end{bmatrix}^T = \bar{\Phi}(\rho)\,\tilde{\Phi}(\rho)\,x$ where $\tilde{\Phi}(\rho)$ is the collection of all local transformations $\tilde{\Phi}$ and $\bar{\Phi}(\rho)$ is the collection of block diagonal matrices stacking the mode-wise local transformations $\bar{\Phi}_i$. This constitutes a parameter-varying output equation but leaves the original states of the system unaltered. The augmented plant is described by the partitioned system

$$\begin{bmatrix} G_\eta \\ G_y \end{bmatrix}_\rho : \begin{cases} \dot{x}(t) = A(\rho(t))\ x(t) + B(\rho(t))\ u(t) \\ \eta(t) = \bar{\Phi}(\rho(t))\,\tilde{\Phi}(\rho(t))\,x(t) \\ y(t) = C(\rho(t))\ x(t) + D(\rho(t))\ u(t)\ . \end{cases} \tag{7}$$

B. Mixed Sensitivity Formulation

A two-degrees-of-freedom controller is used to improve maneuver demand characteristics. Two-degrees-of-freedom controllers can be synthesized in a single step (see e. g. [6]) and are partitioned as

$$u = K_\rho \begin{bmatrix} r \\ y \end{bmatrix} = \begin{bmatrix} K_r & K_y \end{bmatrix}_\rho \begin{bmatrix} r \\ y \end{bmatrix}, \tag{8}$$

where y denotes the measurable output used for feedback control and r denotes a reference command that should not be confused with the yaw rate. A generalized plant P_ρ is constructed such that the interconnection $e = \mathcal{F}_L(P_\rho, K_\rho) \left[\begin{smallmatrix} d \\ r \end{smallmatrix}\right]$

shown in Fig. 2 governs the relation

$$\begin{bmatrix}\tilde{e}_1\\ \tilde{e}_2\\ \tilde{e}_3\end{bmatrix} = \begin{bmatrix}-S\,G_y & S & S_r\\ -T_\mathrm{i} & S_\mathrm{i}\,K_y & S_\mathrm{i}\,K_r\\ G_\eta\,S_\mathrm{i} & G_\eta\,S_\mathrm{i}\,K_y & G_\eta\,S_\mathrm{i}\,K_r\end{bmatrix}\begin{bmatrix}\tilde{d}_1\\ \tilde{d}_2\\ \tilde{r}\end{bmatrix}, \quad (9)$$

where for brevity, the following notation is used:

$$\begin{bmatrix}e_1\\ e_2\\ e_3\end{bmatrix} = \begin{bmatrix}W_{e_1}\,\tilde{e}_1\\ W_{e_2}\,\tilde{e}_2\\ W_{e_3}\,\tilde{e}_3\end{bmatrix}, \qquad \begin{bmatrix}\tilde{d}_1\\ \tilde{d}_2\\ \tilde{r}\end{bmatrix} = \begin{bmatrix}W_{d_1}\,d_1\\ W_{d_2}\,d_2\\ W_r\,r\end{bmatrix}. \quad (10)$$

Clarification of the individual transfer functions is provided in Tab. I. The design task is to select weights that express demands on tracking, disturbance rejection, damping augmentation, robustness and control usage. A static or low-pass weight W_{e_1} sets specifications for tracking bandwidth and disturbance rejection. To provide robustness and to limit control authority, a high-pass weight W_{e_2} is used. A static weight W_{e_3} penalizes peaks in the transfer functions corresponding to excitation of the modal velocities which effectively increases damping of both structural and rigid body modes. Static weights W_{d_1} and W_{d_2} are used to adjust the relative importance of input and output disturbances and hence robustness to uncertainties at either the input or output of the plant. Since feedforward control does not impair robustness, a larger bandwidth is desired in the feedforward path of the controller. The two-degrees-of-freedom formulation allows to achieve this by introducing a low-pass weight W_r that effectively relaxes the roll-off requirement imposed by W_{e_2} for $S_\mathrm{i}\,K_r$. The larger bandwidth leads to improved transient behavior in response to command signals and avoids the induced time delay commonly associated with high-order feedback controllers.

C. Weighting Filter Selection and Tuning

LTI weights are used in order to achieve similar dynamic properties across the flight envelope despite the varying plant dynamics. Still, the filter selection remains non-trivial, interactive and requires a properly scaled plant to start with. Consequently, all input and output channels are normalized with respect to their expected maximum values, as proposed in [6]. The effects of varying the weights are described in Tab. II, although it should be understood that they are not limited to those listed there.

TABLE I
RELEVANT CLOSED-LOOP TRANSFER FUNCTIONS FOR THE DESIGN

Name	Formula
Sensitivity	$S = (I + G_y\,K_y)^{-1}$
Input Sensitivity	$S_\mathrm{i} = (I + K_y\,G_y)^{-1}$
Disturbance Sensitivity	$S\,G_y$
Feedforward Sensitivity	$S_r = I - S\,G_y\,K_r$
Complementary Input Sensitivity	$T_\mathrm{i} = I - S_\mathrm{i}$
Feedback Control Sensitivity	$S_\mathrm{i}\,K_y$
Feedforward Control Sensitivity	$S_\mathrm{i}\,K_r$
Modal Disturbance Sensitivity	$G_\eta\,S_\mathrm{i}$
Modal Complementary Sensitivity	$G_\eta\,S_\mathrm{i}\,K_y$
Modal Feedforward Compl. Sensitivity	$G_\eta\,S_\mathrm{i}\,K_r$

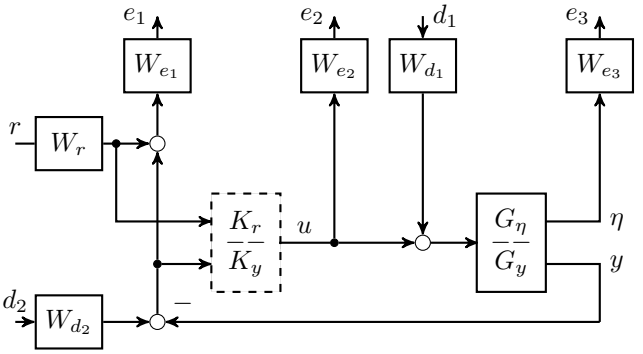

Fig. 2. Feedback interconnection $\mathcal{F}_L(P_\rho, K_\rho)$. The open loop generalized plant P_ρ used for control design is obtained by removing the dashed block.

TABLE II
TUNING KNOBS FOR THE INTEGRATED DESIGN

Tuning	primarily affects	by shaping
W_{e_1}	Tracking, disturbance rejection	S_r, $S\,G_y$
W_{e_2}	Robustness, control effort	$S_\mathrm{i}\,K_y$, $S_\mathrm{i}\,K_r$
W_{e_3}	Damping	$G_\eta\,S_\mathrm{i}\,K_y$
W_{d_1}	Disturbance rejection, damping	$S\,G_y$, $G_\eta\,S_\mathrm{i}$
W_{d_2}	Robustness, control effort	$S_\mathrm{i}\,K_y$
W_r	Tracking, control effort	$S_\mathrm{i}\,K_r$

The present design starts with setting W_{e_1} to enforce a bandwidth of 2 rad/s for roll rate tracking and equal disturbance attenuation for all outputs. The disturbance weights W_{d_1} and W_{d_2} are initially set to $0.2\,I$. The filter W_{e_2} is chosen to loosely represent physical actuator capacities. Weight on the individual channels is then increased until robustness margins at the plant input are satisfied. Next, the weight W_{d_1} is increased until also the output margins are satisfied. Then, W_{e_3} is set to increase dutch roll damping and the damping of the elastic modes. Finally, the weight W_r is adjusted to speed up the response to command signals at the expense of more actuator usage and hence excitation of the elastic modes. The weights that are used in the final design are listed in Tab. III. Static weights satisfy $W = \alpha$. Dynamic weights are of first order and parameterized to satisfy $W(0) = \alpha\,\beta_0$, $|W(\mathrm{j}\,\omega_b)| = \alpha$, and $W(\infty) = \alpha\,\beta_\infty$, i. e., $W(s) = \alpha\,\frac{\beta_\infty\,s + \beta_0\,\omega_b\,\sqrt{(\beta_\infty^2 - 1)/(1 - \beta_0^2)}}{s + \omega_b\,\sqrt{(\beta_\infty^2 - 1)/(1 - \beta_0^2)}}$.

D. Synthesis

The function `lpvsyn` of the recently developed Matlab LPVTools toolbox [20] is used for controller synthesis. It implements Theorem 1 as a convex optimization problem to minimize the performance index γ for systems defined on a parameter grid. A lower bound $\gamma_\mathrm{LTI} = 4.6$ is obtained using `hinfsyn` at each grid point. Achievable performance and computational effort of the LPV synthesis depend on the selection of permissible parameter dependence for X and Y in (5), see Tab. IV. Using affine parameter-dependent matrices significantly improves performance over using constant ones, whereas additional improvement with quadratic dependence is marginal. Hence, an affine dependence is used for the present design. The resultant controller depends on both

TABLE III

WEIGHTING FILTERS FOR INTEGRATED DESIGN

Weight	on	α	β_0	ω_b	β_∞
W_{e_1}	p	1	100	2	0.9
	r, $a_{y,\mathrm{cg}}$, $a_{y,\mathrm{cp}}$	0.9	—	—	—
W_{e_2}	δ_{DH}	2.5	0.5	10	100
	δ_{RL}, δ_{RU}	2	0.5	10	100
	δ_{sp}	1	0.5	10	100
	$\delta_{\mathrm{cv,anti}}$	1	0.5	20	100
W_{e_3}	$\dot{\eta}_{\mathrm{DR}}$	1	—	—	—
	$\dot{\eta}_{\mathrm{E4}}$	10	—	—	—
	$\dot{\eta}_{\mathrm{E5}}$	25	—	—	—
W_{d_1}	all	0.2	—	—	—
W_{d_2}	p	1	—	—	—
	r, $a_{y,\mathrm{cg}}$, $a_{y,\mathrm{cp}}$	0.5	—	—	—
W_r	p	1	7.5	10	0.1

TABLE IV

SYNTHESIS USING DIFFERENT MATRICES X AND Y

Parameter dependence	none	affine	quadratic
Relative performance index $\gamma/\gamma_{\mathrm{LTI}}$	2.50	1.26	1.20
Computation time	12 s	600 s	1800 s

parameters and rates, but to ease implementation, the rate dependence is discarded, i. e., the controller is evaluated for zero rates only. Further, controller dynamics above 150 rad/s are residualized, reducing the controller order from 17 to 13. The fastest remaining mode is then at 50 rad/s, comparable to the classical SAS+SMCS. Validity of these steps is confirmed by examining the controller for different fixed rates and by nonlinear simulation with varying rates. The LPV controller is implemented as a linearly interpolated state space model with its matrices stored in lookup tables.

V. EVALUATION

A roll rate command system designed using classical loopshaping guidelines ([21], [4]) as a lead-compensated PI controller is used for comparison. It is concatenated on the existing gain-scheduled SAS+SMCS of the B-1. Since the SAS acts as an equalizing inner loop, an LTI controller is deemed sufficient for the purpose. Nonlinear simulation with a 10 °/s roll doublet maneuver is performed starting from two different trim conditions: 1) Mach 0.6 at 5,000 ft and 2) Mach 0.8 at 20,000 ft altitude. The goals are to track the roll rate command, to provide turn coordination in terms of sideslip regulation and to avoid structural vibrations. The simulation results are depicted in Fig. 3.

A. Robustness

The controllers are required to achieve minimum linear robustness margins of at least 6 dB gain and 45° phase in accordance with classical design guidelines. The disk margins corresponding to simultaneous gain and phase variations are given in Tab. V for both inputs and outputs with frozen parameters. They are calculated one-loop-at-a-time using Matlab's `loopmargin` function with actuator and servo models in the loop. The margins of the integrated design are similar to the reference design and the robustness criterion is fulfilled for both controllers.

TABLE V

ONE-LOOP-AT-A-TIME DISK GAIN AND PHASE MARGINS

	Conventional Design		Integrated Design	
Input	GM	PM	GM	PM
δ_{DH}	9.8 dB	54°	12.0 dB	61°
δ_{RL}	11.2 dB	59°	10.8 dB	57°
δ_{RU}	∞ dB	90°	10.5 dB	56°
δ_{sp}	14.7 dB	69°	9.0 dB	51°
$\delta_{\mathrm{cv,anti}}$	18.8 dB	76°	27.6 dB	85°
Output	GM	PM	GM	PM
p	7.0 dB	46°	10.7 dB	57°
r	19.9 dB	78°	35.5 dB	88°
$a_{y,\mathrm{cg}}$	11.5 dB	60°	26.2 dB	84°
$a_{y,\mathrm{cp}}$	18.9 dB	77°	10.1 dB	55°

B. Tracking Performance

The responses of the aircraft depicted in Fig. 3a reveal that both controllers achieve a similar roll rate response for both operating points, with the integrated controller reaching the demand value slightly faster than the classical controller. For good handling qualities, responsiveness to pilot commands, i. e., how much a command is delayed by the controller, is even more important. Due to the feedforward path, the integrated controller performs very similar to the classical controller and does not introduce any visible time delay. Turn coordination in terms of sideslip regulation is clearly improved with the integrated controller. Figure 3b shows the corresponding control surface deflections. The integrated controller distributes the control effort different from the conventional design and overall requires less control action during the maneuver. Especially, usage of the control vanes is significantly reduced. Both the improvement in turn coordination and the reduction of required control surface deflections to perform the maneuver show the benefits of jointly using the available effectors in contrast to the conventional design.

C. Damping Augmentation

In Fig. 3c, the acceleration at the cockpit as well as the structural deformation velocities caused by the roll doublet maneuver are depicted. The E_4 mode is shown as the vertical displacement velocity at the wing tip, while the E_5 mode is shown as the lateral displacement velocity at the cockpit.

The two-degrees-of-freedom control structure separately processes the reference signal, which allows the integrated controller to avoid undesired acceleration at the cockpit with a coordinated use of all control surfaces during the maneuver. This is confirmed by Fig. 3c, where cockpit acceleration is clearly reduced by the integrated design in contrast to the conventional one. Further, the deformation velocities decay much faster and the number of load cycles due to oscillation is greatly reduced, which confirms the active damping augmentation through the feedback path of the integrated controller. This combination of active damping and excitation avoidance combined in the integral design is clearly desirable and different from the cancellation of lightly damped modes commonly observed in $\mathcal{H}_\infty$-control.

D. Conclusion

The proposed controller design achieves similar robustness margins and tracking performance with less control effort and improved turn coordination compared to the conventional design. It greatly reduces structural vibrations through a combination of excitation avoidance and active damping augmentation and thus can be concluded to be superior to the conventional design.

Acknowledgment

The authors thank Prof. Schmidt for providing and Arnar Hjartarson for helping with the B-1 simulation. This work was partially supported by NASA STTR contract No. NNXI-ICI09P entitled *Robust Aeroservoelastic Control Utilizing Physics-Based Aerodynamic Sensing* as a subcontract from Tao Systems. Dr. Arun Mangalam is the principal investigator and Dr. Martin Brenner is the NASA technical monitor.

References

[1] M. R. Waszak and D. K. Schmidt, "Flight dynamics of aeroelastic vehicles," *J. Aircraft*, vol. 25, pp. 563–571, 1988.

[2] B. D. Caldwell, R. W. Pratt, R. Taylor, and R. D. Felton, *Flight Control Systems: Practical Issues in Design and Implementation*. Stevenage IET, 2000, ch. Aeroservoelasticity, pp. 225–301.

[3] J. R. Wright and J. E. Cooper, *Introduction to Aircraft Aeroelasticity and Loads*. John Wiley & Sons, 2015.

[4] D. Schmidt, *Modern Flight Dynamics*. New York: McGraw-Hill, 2012.

[5] R. J. Adams, J. M. Buffington, A. G. Sparks, and S. S. Banda, *Robust Multivariable Flight Control*. London: Springer, 1994.

[6] S. Skogestad and I. Postlethwaite, *Multivariable Feedback Control*, 2nd ed. Upper Saddle River, NJ: Prentice Hall, 2005.

[7] S. Bennani, "Robust flight control: Several aeronautical applications," Ph.D. dissertation, Delft University, The Netherlands, 2002.

[8] M. Hanel, "Robust integrated flight and aeroelastic control system design for a large transport aircraft," Ph.D. dissertation, Univ. Stuttgart, Stuttgart, Germany, 2001.

[9] C. van Etten, G. Balas, and S. Bennani, "Linear parametrically varying integrated flight and structural mode control for a flexible aircraft," in *AIAA Conf. Guidance, Navigation, Control*, 1999, pp. 1342–1352.

[10] D. Schmidt, "A nonlinear simulink simulation of a large flexible aircraft," Tech. Rep., 2013. [Online]. Available: http://highered.mcgraw-hill.com/sites/007339811x/student_view0/matlab_files.html

[11] Wykes, Borland, Klepl, and MacMiller, "Design and development of a strutural mode control system," NASA, Tech. Rep. 143846, 1977.

[12] W. J. Rugh and J. S. Shamma, "Research on gain scheduling," *Automatica*, vol. 36, pp. 1401–1425, 2000.

[13] A. Marcos and G. Balas, "Development of linear-parameter-varying models for aircraft," *J. Guidance, Control, Dynamics*, vol. 27, no. 2, pp. 218–228, 2004.

[14] F. Wu, "Control of linear parameter varying systems," Ph.D. dissertation, Univ. California, Berkeley, 1995.

[15] F. Wu, X. Yang, A. Packard, and G. Becker, "Induced $\mathcal{L}_2$-norm control for LPV systems with bounded parameter variation rates," *Int. J. Robust Nonlinear Control*, vol. 6, pp. 2379–2383, 1996.

[16] M. G. Safonov, D. J. N. Limebeer, and R. Y. Chiang, "Simplifying the $\mathcal{H}_\infty$ theory via loopshifting, matrix-pencil and descriptor concepts," *Int. J. Control*, vol. 50, no. 6, pp. 2467–2488, 1989.

[17] A. Hjartarson, P. J. Seiler, and G. J. Balas, "LPV analysis of a gain-scheduled control for an aeroelastic aircraft," in *American Control Conference*, 2014.

[18] T. Kailath, *Linear Systems*. Englewood Cliffs, NJ: Prentice Hall, 1980.

[19] G. D. Wood, "Control of parameter-dependent mechanical systems," Ph.D. dissertation, Univ. Cambridge, 1995.

[20] A. Hjartarson, P. J. Seiler, and G. J. Balas, "LPV aeroservoelastic control using the LPVTools toolbox," in *AIAA Conf. Atmospheric Flight Mechanics*, 2013.

[21] I. Horowitz, *Synthesis of Feedback Systems*. New York: Academic Press, 1963.

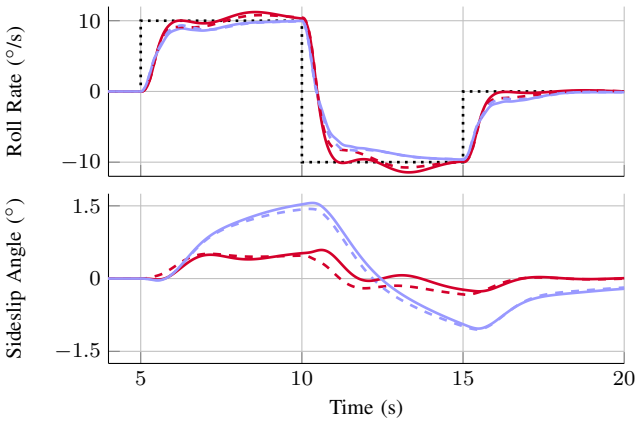

(a) Responses to a roll doublet command (·····)

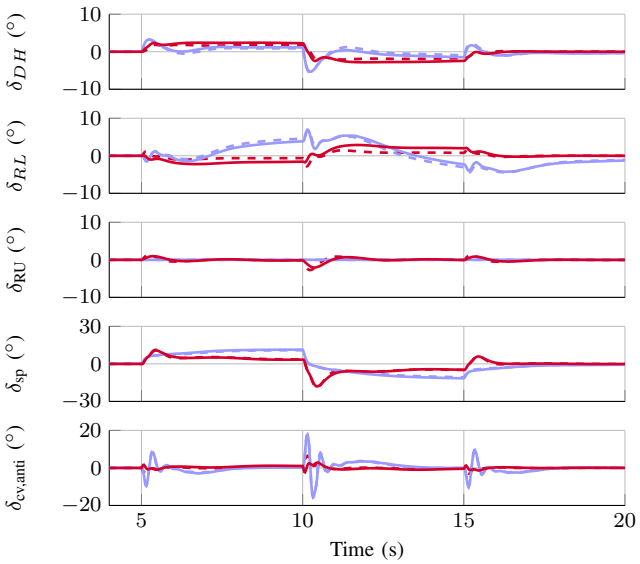

(b) Control surface deflections during the roll doublet maneuver

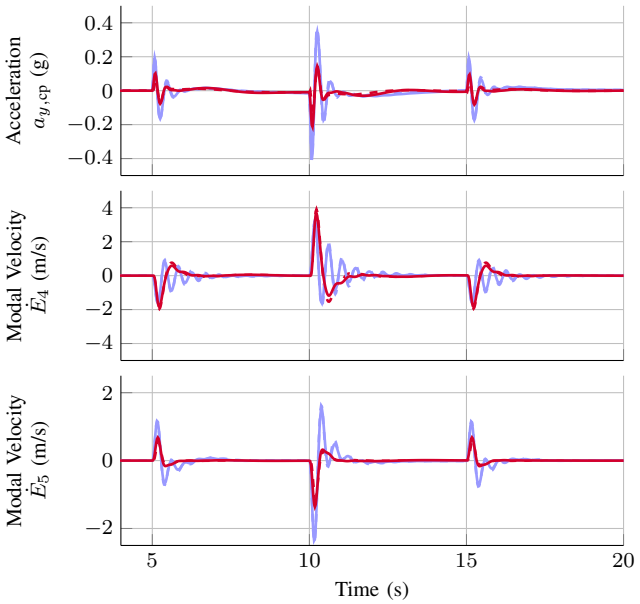

(c) Aeroelastic responses during the roll maneuver

Fig. 3. Nonlinear simulation starting from two different trim conditions: 1) Mach 0.6 at 5,000 ft altitude (integrated ——— and conventional ———), 2) Mach 0.8 at 20,000 ft altitude (integrated - - - and conventional - - -).